Inorganic Chemistry

Article

pubs.acs.org/IC

Temperature Initiated P-Polymerization in Solid $[Cd_3Cu]CuP_{10}$

Melanie Bawohl,[†] Peer Schmidt,*[,‡] and Tom Nilges*[,†]

[†]Department of Chemistry, Synthesis and Characterization of Innovative Materials, Technische Universität München, Lichtenbergstr. 4, 85747 Garching, Germany

[‡]Faculty of Sciences, BTU Cottbus-Senftenberg, Großenhainer Str. 57, 01968 Senftenberg, Germany

Supporting Information

ABSTRACT: $[Cd_3Cu]CuP_{10}$, a polyphosphide containing adamantine-analogue $[P_{10}]$ unit undergoes a solid-state polymerization to form $[P_6]$ rings and tubular $[P_{26}]$ polymer units at elevated temperatures. This reaction represents the rare case of a polyphosphide polymerization in the solid state. The formation of such a polymeric unit starting from a molecular precursor is the first evidence of the general possibility to perform a bottom-up route to the well-known tubular polyphosphide units of elemental phosphorus in a solid material. Temperature-dependent X-ray powder diffraction experiments substantiate the solid phase transformation of $[Cd_3Cu]CuP_{10}$ starting at 550 °C to the polymerized form via an additional intermediate step. A single crystal structure determination of the quenched product at room temperature was performed to evaluate the structural properties and the resulting polyphosphide units. The full polymerization and decomposition mechanism has been analyzed by thermogravimetric experiments and subsequent X-ray powder phase analyses. The present $[P_{26}]$ polymer unit represents a former unseen one-dimensional cut-out of the two-dimensional polyphosphide substructure of Ag_3P_{11} and can be directly related to the tubular polyphosphide substructures of violet or fibrous phosphorus.

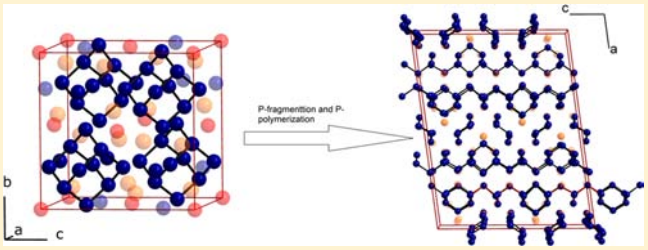

INTRODUCTION

The chemistry of elemental phosphorus is one of the most exciting ones due to the structural variability and the almost endless number of realizable structures.[1] All known allotropes are dominated by covalently bonded substructures resulting in an intriguing variety of reactivity and stability. During the past few years the knowledge in the element chemistry of phosphorus has been significantly increased due to the development of advanced synthesis strategies to prepare new and existing allotropes[2−7] and a thorough evaluation of the energy landscape of stable alloptropes.[8−10] Allotropes of phosphorus such as the red and white varieties have been used for the synthesis of a plethora of new phosphides and polyphosphides to stabilize new anion substructures.[1] In most of the cases, the anion substructure seemed to be generated by a top-down approach cutting the polymeric subunits in defined pieces and rearranging the resulting fragments in various ways. The mineralizer principle for polyphosphides,[11] established for a reasonable number of different polyphosphides, obviously follows the same trend. On variation of the mineralizer reagent, a main group element or d^{10} ion-halide, this mineralizer is capable to activate red phosphorus in such a way that a cascade of polyphosphides with different grades of fragmentation, cation-incorporation to the polymer strands, or rearranged polyanion substructures results. Examples of compounds synthesized using the mineralizer principle are Cu_5InP_{16} with a layered polyphosphide substructure, Cu_2P_{20},[11] $[Au_3Sn]P_7$[12] featuring polymeric phosphorus, or the title compound $[Cd_3Cu]CuP_{10}$.[13] The latter represents one of the smallest molecular (0-dimensional) and closed shell adamantine-like $[P_{10}]$ unit beside the P_4 tetrahedron, prepared by the mineralizer principle. Beside the title compound characterized by closed shell d^{10} cations within the intermetalloid substructure only, a handful of other main group containing adamantane compounds exist. Examples are $[Cu_3Sn]CuP_{10}$,[14] $[Ag_3Sn]CuP_{10}$,[15] and $[Au_3Sn]CuP_{10}$[12] featuring the same polyanionic adamantine-like substructure.

All mentioned compounds have been realized in a top-down approach from amorphous red phosphorus via complex rearrangement processes of larger P-fragments like tubular polymers[16] or polymeric phosphorus linked P_3 triangles and P_4 tetrahedra,[17] which may exist in the molten or solid state. However, a bottom-up approach to polymeric units has been discussed for the reaction of white to red amorphous phosphorus without having a detailed knowledge of the mechanism. Even the transformation of black to violet phosphorus demands the occurrence of complex bond-breaking and -formation processes. To the best of our knowledge, such a bottom-up approach from a small molecular P-unit to a P-polymer strand has not been reported in a pure inorganic material via a solid-state reaction.

The understanding of phase formations and phase transitions in the case of phosphorus chemistry is essential for the understanding of the reactivity of elemental phosphorus and phosphorus compounds with reactive elements like lithium or

Received: June 14, 2013
Published: October 4, 2013

   dx.doi.org/10.1021/ic401508n | Inorg. Chem. 2013, 52, 11895−11901

sodium in conversion and intercalation reactions as well as less reactive elements like tellurium.[18−22] Recently, phosphorus allotropes such as red or orthorhombic black phosphorus gained attention due to their potential as anode material in batteries.[23−25] Reasonable first-cycle capacities of approximately 2500 mAh·g^{-1} and stable capacities of approximately 1800 mAh·g^{-1} have been reported in consecutive cycles. In order to understand this feature, the behavior of phosphorus in direct neighborhood to metals and metalloid cluster compounds will be evaluated.

EXPERIMENTAL SECTION

Synthesis of $[Cd_3Cu]CuP_{10}$. A total amount of 1 g of $[Cd_3Cu]CuP_{10}$ was prepared from a 2/3:3:9 1/3 mixture of Cu_3P, cadmium (Chempur, 99.999%), and phosphorus (Chempur, 99.999%) in evacuated silica ampules. The starting materials were heated within 8 h to 450 °C, kept at that temperature for 19 days, and then cooled to room temperature within 6 h. Cu_3P was prepared prior to use from the elements in ideal ratios in evacuated silica ampules at 550 °C.

Synthesis of Nominal $Cd_{15}Cu_{10}P_{46}$. A phase pure sample of $[Cd_3Cu]CuP_{10}$ (0.150 g) was heated in evacuated silica ampules (lengths 150 mm, inner diameter 10 mm, wall thickness 2 mm) to 500 °C and kept at that temperature for 4 days.

Crystals of $Cd_{15}Cu_{10}P_{46}$ could be separated from the reaction mixture after the above-mentioned treatment. A comparable crystals quality can be achieved by stopping the DTA-TG experiment at 500 °C after a holding period of several hours to allow complete phase transformation.

Energy Dispersive X-ray Spectroscopy (EDX). Semiquantitative elemental analysis was performed with a Leica 420i scanning electron microscope (Zeiss) fitted with an electron-dispersive detector unit (Oxford) and Cd, Cu, and GaP as standards for calibration. A voltage of 20 kV was applied to the samples. All expected elements have been identified in $[Cd_3Cu]CuP_{10}$ and $Cd_{15}Cu_{10}P_{46}$. For nicely shaped $[Cd_3Cu]CuP_{10}$ (see Figure 2), the expected composition was confirmed within the error of the method. Five individual spot measurements have been performed for each crystal on different positions of the crystal surface. The same procedure led to inconsistent results for $Cd_{15}Cu_{10}P_{46}$ due to the highly textured surface of each individual crystal. A metallographic preparation of the sample failed because of the brittleness of the crystals.

Thermogravimetry (TG). TG experiments were performed using a NETZSCH STA 409 Luxx + Äolos under an argon atmosphere. The heating rate during the measurement was set to 10 K·min^{-1}. At the beginning after step 1 and the end step 4 of the thermal decomposition, X-ray powder phase analysis was performed to evaluate the resulting products.

Differential Scanning Calorimetry (DSC). DSC measurements were performed using a Netzsch DSC 204t calorimeter under a nitrogen atmosphere in aluminum crucibles that had a temperature accuracy of ±1 K for onset values. A temperature range of 25−600 °C was applied at a heating rate of 10 K min^{-1} using nitrogen gas atmosphere. At least two consecutive runs were conducted in order to check the reversibility of the observed effects.

Powder X-ray Diffraction (PXRD). A STOE Stadi-P powder diffractometer operated with Mo Kα radiation (λ = 0.71073 Å), fitted with a 130° PSD detector and a STOE-heating unit was used to perform temperature-dependent powder diffraction experiments in a temperature range of 50 to 600 °C. The starting material was transferred to a silica tube of 0.3 mm inner diameter and was kept under an argon atmosphere during the measurements. A data collection was performed every 50 °C up to the maximum temperature of 600 °C and the individual data were collected for 13 h for each temperature step. A temperature ramp of 5 K min^{-1} was used to increase the temperature between the temperature steps.

For phase analytical experiments during and after the DTA-TG measurements, a Stoe Stadi-P powder diffractometer (Cu Kα_1 radiation, λ = 1.54051 Å) fitted with a 5° linear PSD was used to analyze the resulting products.

Single Crystal X-ray Structure Analysis (SXRD). More than 30 different crystals of $Cd_{15}Cu_{10}P_{46}$ have been checked prior to a complete data collection in order to find a suitable one for structure analysis. Intensity data for a structure determination of $Cd_{15}Cu_{10}P_{46}$ were collected on a STOE IPDS-II (Mo K_α radiation, λ = 071073 Å) at 25 °C. According to the metrics of the unit cell and the reflection conditions, three possible space groups *C*2/*m*, *Cm*, and *C*2 were identified as suitable candidates. A chemical meaningful structure model has only been achieved in *C*2. We also tried to solve the structure in the possible rhombohedral space groups (e.g., *R*3*m*), which was also not successful. The best data we could determine showed internal *R* values of 0.1080 and R_σ of 0.2181 applying space group *C*2. We therefore decided to perform an isotropic refinement of most of the positions and only applied harmonic displacement parameters for selected Cu/Cd sites. Details of the crystallographic data and atomic coordinated are summarized in Tables 1 and Table S1 (Supporting Information).

Table 1. Crystallographic Data of $[Cd_3Cu]CuP_{10}$ (Redetermination) and Nominal $Cu_{15}Cd_{10}P_{46}$

compd	$[Cd_3Cu]CuP_{10}$	$Cd_{15}Cu_{10}P_{46}$
molar mass (g mol^{-1})	774.06	
crystal size (mm^3)	0.04 × 0.04 × 0.04	0.04 × 0.02 × 0.02
crystal color	black, isometric	black, fragmented block
crystal system	cubic	monoclinic
space group	$F\bar{4}3m$	*C*2
lattice parameters		
a (Å)	10.479(2)	29.316(5)
b (Å)		7.5519(8)
c (Å)		23.167(4)
β (deg)		97.65(2)
V (Å^3)	1150.7(4)	5083(1)
Z		
ρ_{calc} (g cm^{-3})	4.467	∼4.1
flack	0.47(4)	
diffractometer	STOE IPDS II	
radiation	Mo−Kα (0.71073 Å), graphite monochromator	
absorption correction	numerical	
T (°C)	25	25
independent reflections	212	6411
R_{int} (all)	0.0185	0.108
refinement	least-squares on F^2; JANA2006	
R ($I > 3\sigma I$)	0.0171	0.0738
wR ($I > 3\sigma I$)	0.0462	0.1022
R (all)	0.0173	0.2142
wR (all)	0.0462	0.1224
parameters	14	251
goof (all)	1.79	1.45
residual electron density max/min (e Å^{-3})	1.28/−0.87	3.87/−2.29

A numerical absorption correction was performed prior to the structure refinements based on an optimized crystal shape from symmetry equivalent reflections.[26] Reasonable cell content has been estimated from the thermo-analytic results. The structure was solved using the superflip routine[27] implemented in the Jana2006 program suite.[28] Because of the quality of the single crystals and after the thermal treatment, several constrains and restrictions had to be applied in the structure refinement. Atom positions have been identified according to the underlying electron density and structure chemical considerations. Displacement parameters of the Cd/Cu positions were

dx.doi.org/10.1021/ic401508n | Inorg. Chem. 2013, 52, 11895−11901

refined by a mixed isotropical/harmonic approach. Phosphorus displacement parameters were fixed to reasonable values in some cases. We performed an individual refinement for each Cd/Cu site in order to evaluate the preferred occupancy of one of the elements. After this test, we fixed the occupancy factor of each site to avoid correlations. The polymerization must occur with a complex reorientation of each atom in the structure. Taking the disorder situation in the starting material $[Cd_3Cu]CuP_{10}$ into account, where one Cu site forms the *fcc* latice and the cluster positions are characterized by a 75:25 Cd/Cu positional disorder, this procedure seems to be useful. Because of the overall low crystal quality after the thermal treatment and the loss of P_4 during this process, resulting in high internal *R* values, the refinement of mixed occupied atom positions is not reliable, and a composition has not properly been determined. We therefore decided not to state a refined composition in Table 1. Bond lengths and angles are also not discussed, not neglecting the fact that here some P−P distances in the structure model are too short to be realistic for fully occupied P sites. The P−P bond length distribution ranges from 1.74 Å (P20−P34) to 2.43 Å (P13−P18) of which most P−P distances are in the meaningful region between 2.15 and 2.40 Å. As stated earlier, the suggested structure model can only be a first hint for the realized structure and composition; and additional experiments will have to be performed in order to fully characterize the compound. Nevertheless, X-ray powder diffraction phase analysis based on the suggested structure model (see Figure 1) shows a reasonable agreement between the measured data and the calculated structure model.

RESULTS AND DISCUSSION

There is a strong demand to verify the structural features of noncrystalline materials due to their significance in numerous applications like solar cells,[29] phase change materials,[30] and energy storage applications.[25] White phosphorus with its molecular tetrahedral units can be easily reacted to amorphous red, black, and violet phosphorus via polymerization reactions in the solid state or in the gas phase.[4,5,31,32] Detailed mechanisms of such reactions are missing in the literature. Also the variety of different phosphorus rich polyphosphides prepared from red phosphorus and their often closely related structural features, compared with the crystalline element allotropes, demands a deeper examination of the formation reactions. Herein, we investigated the transformation of an adamantane-like cage to a polymeric unit, a bottom-up approach from simple molecular $[P_{10}]$ to more complex $[P_{26}]$ units. A new tubular polyphosphide results, which is characterized by a unique polyanion substructure and pronounced disorder in the countercation.

$[Cd_3Cu]CuP_{10}$ contains adamantane-like $[P_{10}]$ cages coordinated by metalloid $[Cd_3Cu]$ units and isolated Cu^+ ions.[13] The metalloid $[Cd_3Cu]$ clusters show an orientational disorder characterized by a random orientation of the clusters relative to the $[P_{10}]$ units. As a result, the structure must be described in the space group $F\bar{4}3m$ rather than a lower symmetric one, which can be used to resolve a possible orientation or order of the $[Cd_3Cu]$ clusters (e.g., $R\bar{3}m$). A structure redetermination substantiates this finding and the present structure determination underlines the reported one in the literature. Data are summarized in Table 1. Recently, it was shown in the literature that this disorder behavior is common for all representatives of this class of materials. None of the common structure−analytical methods like X-ray diffraction, solid-state NMR, or other local probe can help to resolve this feature.[15,33−35] Therefore, the starting material and also the starting point of the present polymerization reaction is well-defined concerning the polyphosphide substructure in contrast to a relatively large

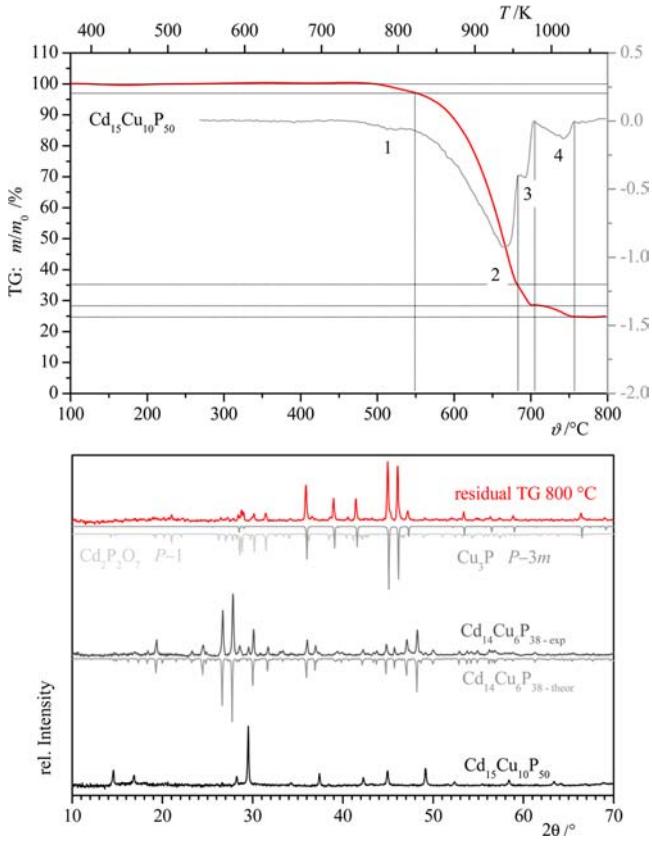

Figure 1. Top: TG results of the four-step reaction of $[Cd_3Cu]CuP_{10}$ to $Cd_{15}Cu_{10}P_{46}$, and the following decomposition via CuP_2 and CuP to the final product Cu_3P. The black curve represents the 1st derivative of the TG curve (DTG) where 1 to 4 denote the different steps of decomposition and phase formation upon heating. Bottom: Powder-XRD of the initial compound $[Cd_3Cu]CuP_{10}$ = $Cd_{15}Cu_{10}P_{50}$ (bottom), $Cd_{14}Cu_6P_{38}$, the product of thermal decomposition in step 1 (middle), and the final product Cu_3P of step 4 (STOE StadiP). A small intake of oxygen during the TG experiment led to the formation of $Cd_2P_2O_7$,[36] which has been identified by the powder pattern.

set of different possible coordination modes of the cluster atoms relative to the P_{10} unit. As shown recently for $[Au_3Sn]P_7$ and $[Cu_3Sn]CuP_{10}$, such an arrangement is characterized by a low effective positive charge on each cluster position,[36,37] and therefore, a weak interaction can be estimated for the present cluster to the neighboring $[P_{10}]$ units.

During our thermoanalytical investigation of $[Cd_3Cu]CuP_{10}$, a complex thermal behavior was observed, which is in contrast to all other known phases in this system.[13] While all other representatives of this class of materials decompose to binary phases at elevated temperatures, the title compound shows a different behavior. The adamantine-like polyphosphide substructure is fragmented and polymerized afterward. Details of the performed TG analyses are summarized in Figure 1 and Table 2.

At an onset temperature of 470 °C, a mass loss equivalent to one P_4 molecule has been found, which indicates the beginning of a solid state reaction of the starting material. We have stopped the reaction shortly above this feature at approximately 500 °C and isolated the reaction products for further analysis. Figure 2 shows the morphology of crystals of the starting material and the product isolated after the first reaction step. Upon further heating, a second mass loss starts at 540 °C where

dx.doi.org/10.1021/ic401508n | Inorg. Chem. 2013, 52, 11895−11901

Table 2. TG Results for Decomposition Reaction of Cadmium Copper Phosphide $[Cd_3Cu]CuP_{10}$ in Calculation of the Decomposition Mechanism Towards Cu_3P and $Cd_2P_2O_7$, as Observed in the Residue of the TG Experiment; the EDX Results Are Normalized on an Ideal P-Content According the Expected Sum Formula; the Calculation of the Oxygen Intake Is Given in Line 4

product	decomposition reaction	composition EDX	T_{onset} (°C)	TG range (°C)	theor mass loss (%)	exptl mass loss (%)
$[Cd_3Cu]CuP_{10} = Cd_{15}Cu_{10}P_{50}$		Cd/Cu/P 16(1):11(1):50(1)				
	$- P_{4(g)}$		470(2)	470 − 540	−3.2	−3.1(5)
$Cd_{15}Cu_{10}P_{46}$		Cd/Cu/P 22(1):3(1):46(1)				
	$- 6.25P_{4(g)}$ $- 14Cd_{(g)}$ $+ 7/4O_{2(g)}$		540(2)	540 − 685	−59.2	−61.7(10)
$10CuP_2$ $+ 1/2Cd_2P_2O_7$						
	$- 2.5P_{4(g)}$		685(2)	685 − 705	−8.0	−7.1(10)
10 CuP $+ 1/2Cd_2P_2O_7$						
	$- 5/3P_{4(g)}$		705(2)	705 - 755	−5.3	−3.6(10)
$10/3Cu_3P$ $+ 1/2Cd_2P_2O_7$					Σ = −75.7	−75.5(10)

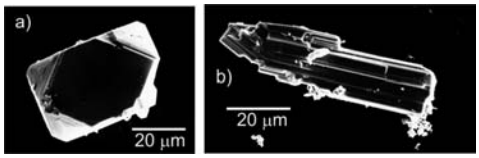

Figure 2. Representative crystals of (a) $[Cd_3Cu]CuP_{10}$ (= $Cd_{15}Cu_{10}P_{50}$) and (b) $Cd_{15}Cu_{10}P_{46}$ (composition from X-ray data, $Cd_{14}Cu_6P_{38}$), the reaction product after the loss of one equivalent of P_4 per formula unit. Obviously, the P_4-loss results in strong texturing of the remaining crystals. Crystals are fragmented during the phase formation due to the loss of P_4.

additional phosphorus and cadmium evaporates. A total mass loss of 62(1) % up to 685 °C is consistent with the formation of CuP_2, followed by an intermediate phase with the nominal composition CuP, formed between 685 and 705 °C. In a last step above 705 K, the final product Cu_3P is formed.

On the basis of the initial composition $[Cd_3Cu]CuP_{10}$ (=$Cd_{15}Cu_{10}P_{50}$) and the mass loss of 3.1% during the thermal treatment (which is related to P_4 molecule), the intermediate compound must be formulated as $Cd_{15}Cu_{10}P_{46}$. The second step almost immediately follows the first one. Thus, a small amount of further loss of phosphorus can lead to the formation of slightly different phase compositions. The intermediate phase and final product of the decomposition Cu_3P has been identified by X-ray powder phase analysis (Figure 1). All decomposition temperatures and areas of stability are denoted in Table 2. The unwanted intake of traces of oxygen via the inert gas during the DTA-TG experiment led to the formation of $Cd_2P_2O_7$.[36] If this formation was added to the calculation of the overall mass balance in the TG experiment, the theoretical and experimental mass losses coincide to each other (Table 2, line 3).

Obviously, the weak interaction of the clusters to the polyphosphides is a reasonable and important feature at the beginning of a solid state decomposition-reaction at elevated temperatures. In all known cases where a main group element like Sn is present in the cluster, such behavior could not be observed. Therefore, the question arises what kind of reaction may take place after the loss of one equivalent of P_4. SEM images of representative crystals of $[Cd_3Cu]CuP_{10}$ and nominal $Cd_{15}Cu_{10}P_{46}$, the reaction product after the P_4 loss, are given in Figure 2. The morphology of $Cd_{15}Cu_{10}P_{46}$ points toward a severe effect on the crystals during reaction.

A single crystal structure determination of the reaction product after the first step in the DTA-TG experiment was performed after the reaction mixture was cooled down to room temperature. A brief overview on the polyphosphide substructures of $[Cd_3Cu]CuP_{10}$ and nominal $Cd_{15}Cu_{10}P_{46}$ is given in Figure 3.

In addition to the loss of P_4, the evaporation of Cd, initiated shortly after the loss of P_4, is also a critical feature for the isolation of well-defined crystals for single crystal structure determination. We cannot derive or estimate the expected composition from the underlying starting material due to this possible Cd evaporation at elevated temperatures. It is probable that the composition of each crystal can vary slightly with increasing temperature. Therefore, the cation ratio can vary for each single measurement and is strongly dependent on the history of each crystal. This feature has to be taken into account when the quality and information content of the structure determination is evaluated. The following structure model can therefore be not more than a first impression of the structure, realized after P_4 loss. Details concerning the refinement procedure and the used constraints and restraints are given in the experimental section. Because of the quality of the refinement data, a deeper discussion of bond lengths and angles will be completely neglected. Nevertheless, the underlying process for the formation of this phase can be derived from these data.

The former molecular-like adamantane-type substructure has been rearranged to form chair-like $[P_6]$ rings and a polymeric $[P_{26}]$ unit built up by comparable $[P_6]$ rings and screwed $[P_7]$ chains, as stated before. A probable dissociation−polymerization mechanism upon heating can be estimated by three relatively simple fragmentations of the $[P_{10}]$ units in $[Cd_3Cu]$-CuP_{10}. The $[P_6]$ rings can be directly formed via a fragmentation of the $[P_{10}]$ units (Figure 3, green ellipse). All $[P_6]$ ring atoms are almost invariant in position, bond length, and bond angles. Only two more fragmentation scenarios, followed by a slight dislocation of some of the atoms, are necessary to explain the formation of the $[P_{26}]$ units (red ellipse

dx.doi.org/10.1021/ic401508n | Inorg. Chem. 2013, 52, 11895−11901

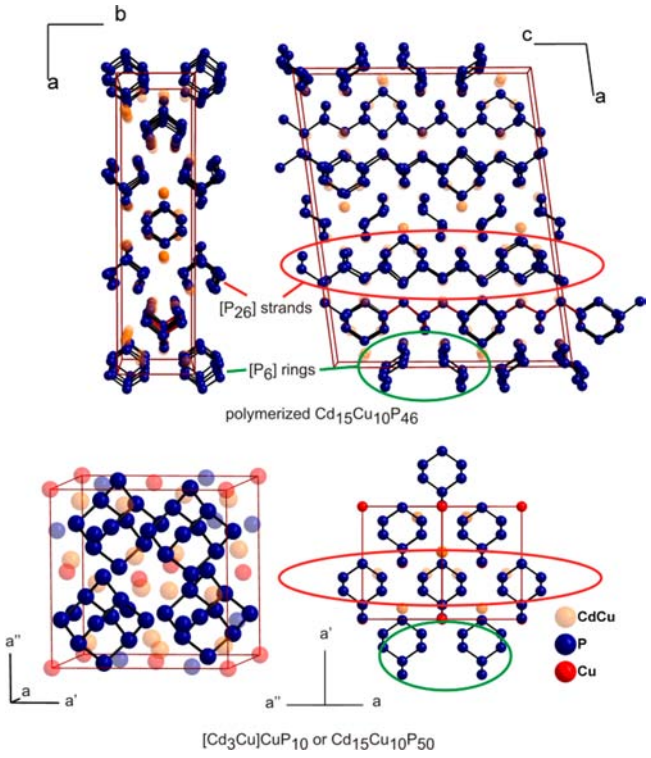

Figure 3. Top part: Crystal structure sections of $Cd_{15}Cu_{10}P_{46}$; view parallel and perpendicular to the $[P_{26}]$ strands (marked by a red ellipse) and $[P_6]$ rings (green ellipse). Bottom part: Crystal structure sections of the starting material $[Cd_3Cu]CuP_{10}$ ($Cd_{15}Cu_{10}P_{50}$), space group $F\bar{4}3m$, a = 10.479(2) Å. The unit cell contains adamantine-like $[P_{10}]$ units (emphasized) embedded in a *fcc* cation substructure formed by Cu. Cu and Cd are forming metalloid $[Cd_3Cu]$ tetrahedral, occupying all octahedral voids of the *fcc* lattice (not shown). Cell edges are drawn in dark red. Similar structure sections in $[Cd_3Cu]CuP_{10}$ forming the polyanion substructure in $Cd_{15}Cu_{10}P_{46}$ are marked with ellipsoids.

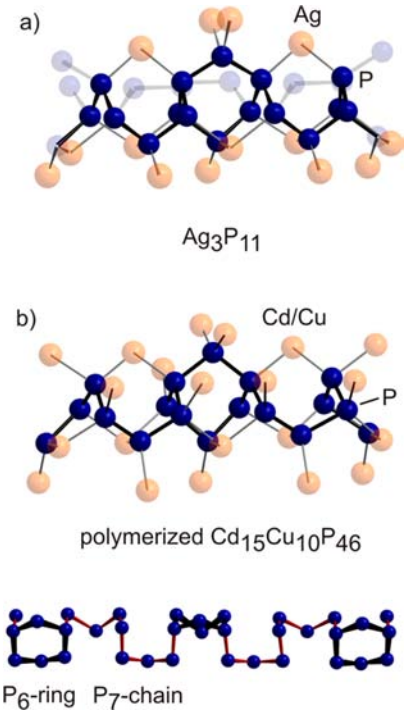

Figure 4. Structure sections of (a) Ag_3P_{11}[37] and (b) $Cd_{15}Cu_{10}P_{46}$, featuring the first coordination spheres around the polyanionic substructures. The 2-dimensional polyphosphide substructure of Ag_3P_{11} is illustrated by solid and transparent blue spheres. To derive the structure of $Cd_{15}Cu_{10}P_{46}$, some of the P-positions in the polyanion substructure of Ag_3P_{11} are substituted by cations to form the new $[P_{26}]$ unit. The $[P_{26}]$ unit (shown below the structure section b) can be regarded as $[P_6]$ rings (emphasized with bold black lines) in chair conformation coordinated by screwed $[P_7]$ chains (red lines).

in Figure 3). A close structure relationship to Ag_3P_{11}[37] is present. The polyanion substructure of $Cd_{15}Cu_{10}P_{46}$ must be regarded as the 1-dimensional (1-D) derivative of the 2-dimensional (2-D) polyphosphide substructure of Ag_3P_{11} (see Figure 4).

Some of the cross-linking P positions in the polyphosphide substructure of Ag_3P_{11} are formally substituted by cations to realize the $[P_{26}]$ polymer unit in $Cd_{15}Cu_{10}P_{46}$. From a structure chemical point of view, the metal-ion substitution grade in the polyphosphide substructure is significantly enhanced in the title compound compared with Ag_3P_{11}.

The Cd and Cu substructures of the starting material $[Cd_3Cu]CuP_{10}$ has been characterized by orientationally disordered metalloid $[Cd_3Cu]$ tetrahedra, which have been proven earlier on in the literature.[23] Because of the high Cu ion mobility and the tendency of Cd to evaporate at the temperatures of phase formation, a strong disorder can be expected for the Cu and Cd substructure in the new compound. Exactly such behavior is observed and represented in the structure model causing severe problems. Almost every Cd/Cu position has to be refined with an occupation disorder for both elements. In the present case, based on the data quality and the suggested structure model, it is not possible to refine the composition properly.

A final proof of the suggested decomposition/polymerization mechanism has to be worked out by additional experiments, but on the basis of the presented data, this mechanism is at least highly probable.

In order to follow the phase formation in situ and to get a first impression on the transformation speed, a temperature-dependent X-ray powder experiment was performed (Figure 5). The phase transition from cubic $[Cd_3Cu]CuP_{10}$ to monoclinic $Cd_{15}Cu_{10}P_{46}$ starts around 500 °C in good agreement with the observation in TGA experiments. An intermediate, but unidentified, phase occurs at this temperature characterized by additional reflections in the powder pattern. At about 550 °C, the polymerization process and rearrangement of the adamantane substructure takes place leading to the formation of $Cd_{15}Cu_{10}P_{46}$ close to 600 °C. We stopped the reaction at this temperature in order to avoid the evaporation of Cd upon further heating. Because of a slow polymerization process, the transformation from $[Cd_3Cu]CuP_{10}$ to $Cd_{15}Cu_{10}P_{46}$ has not been completed, even after several hours of experiment time. Both phases are present at room temperature after cooling. Nevertheless, the irreversibility of the polymerization is obvious. $Cd_{15}Cu_{10}P_{46}$ has not been depolymerized to the starting material. We finalized the polymerization by an additional tempering step for 2 days at 600 °C, after the temperature-dependent X-ray diffraction experiment. The diffraction pattern of the product is included in Figure 5. This finding also substantiates the irreversible loss of material (in this case the identified P_4) during the reaction.

A schematic representation of fragments that polymerize to the final product is given in Figure 5. Green and pink spheres form the $[P_6]$ rings and the $[P_{26}]$ units, while the turquoise

dx.doi.org/10.1021/ic401508n | *Inorg. Chem.* 2013, 52, 11895−11901

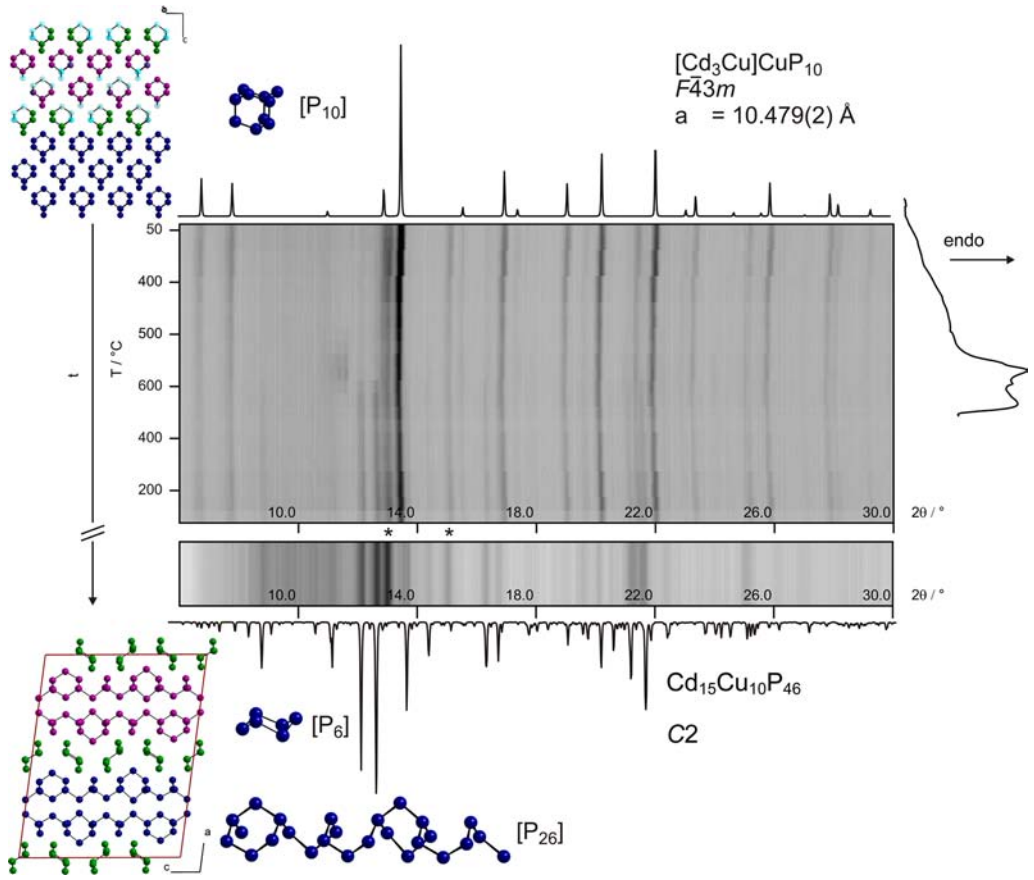

Figure 5. Results from temperature-dependent X-ray powder diffraction and DSC experiments on $[Cd_3Cu]CuP_{10}$. Sections of the respective polyanion substructures of $[Cd_3Cu]CuP_{10}$ and the polymerization product are given on the left-hand side. Different colors in the upper part of the image denote the fragments that polymerize in the final product. The X-ray powder patterns are performed every 50 °C, and a DSC measurement featuring endothermic effects is shown on the right-hand side for comparison. $[Cd_3Cu]CuP_{10}$ was reacted to the polymerized form via an intermediate crystalline phase at 550 °C. The slow polymerization reaction of $[Cd_3Cu]CuP_{10}$ was not finished during the X-ray experiment, and a full transformation was substantiated by a subsequent thermal treatment at 600 °C for 2 days. The formation of an intermediate compound and the final polymerization product is accompanied by two endothermic DSC effects. X-ray pattern are calculated for $[Cd_3Cu]CuP_{10}$ and the polymerization product from single crystal X-ray data.

spheres are supposed to be the ones to form the evaporating $[P_4]$ units.

CONCLUSIONS

$[Cd_3Cu]CuP_{10}$ is a member of a structure family containing an adamantine-like polyphosphide and metalloid $[Cd_3Cu]$ cluster. A detailed thermoanalytical and structure chemical investigation has been performed, which proved the occurrence of a former unseen fragmentation and polymerization reaction of molecular adamantine-like $[P_{10}]$ units to smaller $[P_6]$ rings and a new polymeric $[P_{26}]$ polyanion in $Cd_{15}Cu_{10}P_{46}$. To the best of our knowledge, the $[P_{26}]$ unit is a new polyanionic species, which adds one additional structure motive to the intriguing and rich family of polyphosphides. The formation of those polyanionic units was initiated by controlled heating of $[Cd_3Cu]CuP_{10}$ to elevated temperatures. The polymerization is irreversible and comes alongside with a pronounced texturing of the resulting crystals after the evaporation of P_4 molecules. A full thermal decomposition of the starting material was initiated, which resulted in Cu_3P as the final product. Phosphorus and cadmium are evaporating as the bulk material during heat treatment.

ASSOCIATED CONTENT

Supporting Information

Crystallographic information files (CIF) of $[Cd_3Cu]CuP_{10}$ and nominal $Cd_{15}Cu_{10}P_{46}$. Table with Atomic coordinates and isotropic displacement parameters of $[Cd_3Cu]CuP_{10}$ and nominal $Cd_{15}Cu_{10}P_{46}$ at 25 °C. This material is available free of charge via the Internet at http://pubs.acs.org.

AUTHOR INFORMATION

Corresponding Authors

*(P.S.) Tel: +49 (0)3573 85827. Fax: +49 (0)3573 85809. E-mail: peer.schmidt@hs-lausitz.de.

*(T.N.) Tel: +49 (0)89 289 13110. Fax: +49 (0)89 289 13762. E-mail: tom.nilges@lrz.tum.de.

Notes

The authors declare no competing financial interest.

ACKNOWLEDGMENTS

This work was gratefully financed by the DFG with the grants NI 1095/1-1, NI 1095/1-2, and Schm1616/3 (Priority research program 1415 of the DFG). The contribution of H. Dallmann (Inorganic Chemistry, Dresden University of Technology) is

gratefully acknowledged for the performance of thermogravimetric analyses.

REFERENCES

(1) Pöttgen, R.; Hönle, W.; von Schnering, H. G. In *Encyclopedia of Inorganic Chemistry*, 2nd ed.; King, R. B., Ed.; Wiley: Chichester, U.K., 2005; Vol. *VIII*, p 4268.
(2) Ruck, M.; Hoppe, D.; Wahl, B.; Simon, P.; Wang, Y.; Seifert, G. *Angew. Chem.* **2005**, *117*, 7788; *Angew. Chem., Int. Ed.* **2005**, *44*, 7616.
(3) Pfitzner, A.; Bräu, M. F.; Zweck, J.; Brunklaus, G.; Eckert, H. *Angew. Chem.* **2004**, *116*, 4324; *Angew. Chem., Int. Ed.* **2004**, *43*, 4228.
(4) Lange, S.; Schmidt, P.; Nilges, T. *Inorg. Chem.* **2007**, *46*, 4028.
(5) Nilges, T.; Kersting, M.; Pfeifer, T. *J. Solid State Chem.* **2008**, *181*, 1707.
(6) Osters, O.; Nilges, T.; Bachhuber, F.; Pielnhofer, F.; Weihrich, R.; Schöneich, M.; Schmidt, P. *Angew. Chem.* **2012**, *124*, 3049; *Angew. Chem., Int. Ed.* **2012**, *51*, 2994.
(7) Schmidt, P.; Schöneich, M.; Bawohl, M.; Nilges, T.; Weihrich, R. *J. Thermal Anal. Calorim.* **2012**, *110*, 1511.
(8) Karttunen, A. J.; Linnolahti, M.; Pakkanen, T. A. *Chem.—Eur. J.* **2007**, *13*, 5232.
(9) Karttunen, A. J.; Linnolahti, M.; Pakkanen, T. A. *ChemPhysChem* **2008**, *9*, 2550.
(10) Nava, P.; Ahlrichs, R. *Chem.—Eur. J.* **2008**, *14*, 4039.
(11) Lange, S.; Bawohl, M.; Weihrich, R.; Nilges, T. *Angew. Chem.* **2008**, *120*, 5736; *Angew. Chem., Int. Ed.* **2008**, *47*, 5654.
(12) Lange, S.; Nilges, T. *Z. Naturforsch.* **2006**, *61b*, 871.
(13) Bawohl, M.; Nilges, T. *Z. Anorg. Allg. Chem.* **2009**, *635*, 667.
(14) Hönle, W.; von Schnering, H. G. *Z. Kristallogr.* **1980**, *153*, 339.
(15) Lange, S.; Sebastian, C. P.; Zhang, L.; Eckert, H.; Nilges, T. *Inorg. Chem.* **2006**, *45*, 5878.
(16) Fasol, G.; Cardona, W.; Hönle, W.; von Schnering, H. G. *Solid State Commun.* **1984**, *52*, 307.
(17) Zaug, J. M.; Soper, A. K.; Clark, S. M. *Nat. Mater.* **2008**, *7*, 890–899.
(18) Schmidt, P.; Binnewies, M.; Glaum, R.; Schmidt, M.; Chemical Vapor Transport Reactions: Methods, Materials, Modeling. In: *Advanced Topics on Crystal Growth*; InTech: Rijeka, Croatia, 2013.
(19) Philipp, F.; Schmidt, P.; Milke, E.; Binnewies, M.; Hoffmann, St. *J. Solid State Chem.* **2008**, *181*, 2859.
(20) Philipp, F.; Schmidt, P.; Ruck, M.; Schnelle, W.; Isaeva, A. *J. Solid State Chem.* **2008**, *181*, 2859.
(21) Tschulik, K.; Ruck, M.; Binnewies, M.; Milke, E.; Hoffmann, S.; Schnelle, W.; Fokwa, B. P. T.; Gillesen, M.; Schmidt, P. *Eur. J. Inorg. Chem.* **2009**, , 3102.
(22) Tschulik, K.; Hoffmann, St.; Fokwa, B. P. T.; Gillesen, M.; Schmidt, P. *Solid State Sci.* **2010**, *12*, 2030.
(23) Marino, C.; Debenedetti, A.; Fraisse, B.; Favier, F.; Monconduit, L. *Electrochem. Commun.* **2011**, *13*, 346.
(24) Sun, L.-Q.; Li, M.-J.; Sun, K.; Yu, S.-H.; Wang, R.-S.; Xie, H.-M. *J. Phys. Chem. C* **2012**, *116*, 14772.
(25) Stan, M. C.; von Zamory, J.; Passerini, S.; Nilges, T.; Winter, M. *J. Mater. Chem. A* **2013**, *1*, 5293.
(26) *XArea*, Version1.56; STOE & Cie GmbH: Darmstadt, Germany, 2011
(27) Palatinus, L.; Chapuis, G. *J. Appl. Crystallogr.* **2007**, *40*, 786.
(28) Petricek, V.; Dusek, M.; Palatinus, L. *Jana2006*, the crystallographic computing system; Institute of Physics: Praha, Czech Republic, 2006.
(29) Tawada, Y.; Tsuge, K.; Kondo, M.; Okamoto, H.; Hamakawa, Y. *J. Appl. Phys.* **1982**, *53*, 5273.
(30) Buller, S.; Koch, C.; Bensch, W.; Zalden, P.; Sittner, R.; Kremers, S.; Wuttig, M.; Schürmann, U.; Kienle, L.; Leichtweiß, T.; Janek, J.; Schönborn, B. *Chem. Mater.* **2012**, *24*, 3582.
(31) Hittorf, W. *Ann. Phys. Chem.* **1865**, *126*, 193.
(32) Hultgren, R.; Gingrich, N. S.; Warren, B. E. *J. Chem. Phys.* **1935**, *3*, 351.
(33) Goryunova, N. A.; Orlov, V. M.; Sokolova, V. I.; Shepenkov, G. P.; Tsvetkova, E. V. *Phys. Status Solidi A* **1970**, *3*, 75.
(34) Bullet, D. W.; Dawson, W. G. *Solid State Commun.* **1986**, *60*, 767.
(35) Weihrich, R.; Lange, S.; Nilges, T. *Solid State Sci.* **2009**, *11*, 519.
(36) Calvo, C.; Au, P. K. L. *Can. J. Chem.* **1969**, *47*, 3409.
(37) Möller, M. H.; Jeitschko, W. *Inorg. Chem.* **1981**, *20*, 828.